Radiation torque on a birefringent sphere caused by an electromagnetic wave

Mengkun Liu,[1] Nian Ji,[1] Zhifang Lin,[2] and S. T. Chui[3]
[1]*Surface Physics Laboratory and Department of Physics, Fudan University, Shanghai 200433, China*
[2]*Department of Physics, Fudan University, Shanghai 200433, China*
[3]*Bartol Research Institute, University of Delaware, Newark, Delaware 19716, USA*
(Received 25 March 2005; published 23 November 2005)

We present an exact *ab initio* calculation of the optical torque on a spherical uniaxially birefringent particle of arbitrary size illuminated by plane electromagnetic wave of arbitrary polarization mode and direction of propagation. The calculation is based on the extended Mie theory and the Maxwell stress tensor formalism. The expression for evaluating radiation torque is derived for arbitrary (absorbing and lossless) isotropic surrounding medium. The dependence of the optical torque on the incident angle, the polarization mode, the material birefringence, as well as the particle size, has been systematically investigated. For normal illumination, namely, with the incident wave vector $\mathbf{k}_0$ perpendicular to the extraordinary axis (EA) of the particle, the optical torque Γ caused by a linearly polarized (LP) incident wave always shows the angle dependence $\Gamma = \Gamma_0 \sin 2\varphi_e$. Here, φ_e is the angle between the EA and the incident electric field, whereas Γ_0 may take positive or negative values, dependent on n_e, n_o, and the particle size. In the small particle limit, Γ versus particle radius a displays different power law behaviors, $\Gamma \sim a^3$ and $\Gamma \sim a^6$, for LP and circularly polarized (CP) incident waves, respectively, while for small material birefringence $|\Delta n| = |n_e - n_o|$, linear and square laws, $\Gamma \sim |\Delta n|$ and $\Gamma \sim |\Delta n|^2$, are found for the LP and the CP incident modes, respectively.

DOI: 10.1103/PhysRevE.72.056610 PACS number(s): 41.20.−q, 87.80.Cc, 42.62.−b, 78.20.Fm

I. INTRODUCTION

It is well known that electromagnetic wave transports angular momentum as well as linear momentum. When scattered, in addition to optical force caused by the transfer of linear momentum, the electromagnetic wave also exerts on the scatterer a torque due to the transfer of angular momentum. In a certain case, this torque may make the scatterer rotate [1], which, when combined with optical tweezers [2], introduces a unique and simple handle to control both the location and the orientation of a particular microsized particle. The advance has led to a wide variety of applications, including the possibility of rotating biological structure and developing optically driven and controlled micromachines. It has been shown [3] that the optical torque would vanish for an isotropic nonabsorbing spherical scatterer. So, early rotational micromanipulation was achieved by using absorbing particles [4,5]. To overcome the heating problem in the absorbing particle that limits the achievable rotation rate, optical systems have recently been designed with lossless geometrically anisotropic [6–11] and optically anisotropic (birefringent) particles [12–19]. In particular, optical apparatuses have been demonstrated [18,19] that can apply and accurately measure the torque exerted by laser beam on a birefringent particle.

Although intensively investigated experimentally, the optical torque on a birefringent particle was theoretically evaluated mostly in two limiting cases: $\lambda \ll a$ [12,20] and $\lambda \gg a$ [18]. Here, λ denotes the incident wavelength, and a the dimension of the scattering particle, e.g., the radius of spherical scatterer. Friese and co-workers [12] proposed that the optical torque per unit area is given by

$$\Gamma = -\frac{\epsilon c}{2\omega} E_0^2 \sin[k_0 d(n_o - n_e)] \cos 2\phi \sin 2\varphi_e + \frac{\epsilon c}{2\omega} E_0^2 \{1 - \cos[k_0 d(n_o - n_e)]\} \sin 2\phi, \tag{1}$$

where ϵ is the electric permittivity, k_0 the free-space wave number, ω the angular frequency of incident wave, c the light velocity, d the thickness of the particle, and n_o and n_e are the refractive indices of the birefringent particle in, respectively, the ordinary and extraordinary directions, whereas φ_e is the angle between the extraordinary axis (EA) of the birefringent particle and the incident electric field, and finally, ϕ describes the degree of ellipticity of the incident light [12], with $\phi = 0$ or $\pi/2$ corresponding to linearly polarized (LP) and $\phi = \pi/4$ circularly polarized (CP) light. The expression, ideally suited for a flat disk, is based on ray optics, which is valid in the limiting case $\lambda \ll a$. La Porta and Wang presented another expression [18], which was implicit in the earlier analysis of more elementary cases (see, e.g., Ref. [3])

$$\Gamma = \hat{q} \Gamma_0 \sin 2\varphi_e, \tag{2}$$

where $\hat{q}$ is a unit vector normal to the electric field and the polarization induced on the scatterer, and Γ_0 is the maximum magnitude of the optical torque. Equation (2) was derived in the limiting case $\lambda \gg a$. The two expressions meet difficulty for the intermediate case, where the size of the scattering particle a and the incident wavelength λ are of the same order. It is therefore desirable to have a complete solution to the optical torque problem on birefringent particle.

The purpose of this paper is to present an exact *ab initio* calculation of the radiation torque on a spherical uniaxially birefringent particle of arbitrary size, caused by an incident plane electromagnetic wave with arbitrary polarization mode and direction of propagation. The dependence of the radiation torque on the incident angle, incident polarization mode, incident wavelength, as well as the material birefringence has been systematically investigated. The results verify the wave-plate behavior in the transfer of angular momentum from light to the scatterer. It is found that the angle dependence of Eq. (2), which is derived in the limiting case $\lambda \gg a$, remains valid for arbitrary particle size when the particle is subject to normal illumination, namely, with the incident wave vector $\mathbf{k}_0$ normal to the EA, by the LP incident wave. However, the maximum magnitude Γ_0 of the optical torque may change sign as particle size increases, in qualitative agreement with the first term of Eq. (1) derived based on ray optics. Due to the shape effect, at some particular ranges of particle size, the EA can be aligned by the LP incidence with the E-field direction regardless of $n_e - n_o = \pm|\Delta n|$, presenting a striking contrast to Eq. (1), since the latter implies that, for the LP incidence, particles with $n_e - n_o = |\Delta n|$ and $n_e - n_o = -|\Delta n|$ are always subject to torque in opposite directions. For different polarization modes of the incident plane wave, the radiation torque Γ versus the particle radius a may display different power-law behaviors in the small particle limit. In addition, the torque is found to exhibit linear and square law dependence on the material birefringence $\Delta n = n_e - n_o$ for small $|\Delta n|$, regardless of the particle size.

The rest of the paper is organized as follows. In Sec. II, we describe a comprehensive formulation of exact *ab initio* calculation of radiation torque based on the Mie-type solution and the Maxwell stress tensor formalism. Systematic numerical results are presented in Sec. III. A summary is given in Sec. IV. Some technical results are relegated to the Appendix.

II. GENERAL FORMULATION

The Mie-type solution to the scattering problem of plane electromagnetic waves by a sphere of arbitrary size and with gyromagnetic permeability tensor has recently been presented [21]. Here, we first outline the scheme of the solution to the scattering problem and then concentrate on the derivation of the radiation torque formulas based on the Maxwell stress tensor formalism.

A. Mie-type solution of scattering by a birefringent sphere

The Maxwell equations for time-harmonic field inside the sourceless and homogeneous spherical particle read (assuming time dependence $e^{-i\omega t}$)

$$\nabla \times \mathbf{E}_I = i\omega \mathbf{B}_I, \tag{3a}$$

$$\nabla \times \mathbf{H}_I = -i\omega \mathbf{D}_I, \tag{3b}$$

$$\nabla \cdot \mathbf{D}_I = 0, \tag{3c}$$

$$\nabla \cdot \mathbf{B}_I = 0. \tag{3d}$$

The constitutive relations between the electric displacement vector $\mathbf{D}_I$, the magnetic induction $\mathbf{B}_I$, the electric field $\mathbf{E}_I$, and the magnetic field $\mathbf{H}_I$ inside the particle are given, for a birefringent particle, by

$$\mathbf{D}_I = \epsilon_s \overleftrightarrow{\epsilon} \cdot \mathbf{E}_I, \quad \mathbf{B}_I = \mu_s \mathbf{H}_I, \tag{4}$$

where the permittivity tensor $\epsilon_s \overleftrightarrow{\epsilon}$ is given by

$$\epsilon_s \overleftrightarrow{\epsilon} = \epsilon_s \begin{pmatrix} 1 & 0 & 0 \\ 0 & 1 & 0 \\ 0 & 0 & 1+u \end{pmatrix}, \tag{5}$$

and $\epsilon_s(\mu_s)$ is the scalar permittivity (permeability). For simplicity, μ_s is set to be μ_0, the permeability of the surrounding medium, while $\epsilon_s = \epsilon_r \epsilon_0$, with ϵ_0 denoting the permittivity outside particle. It follows from (3) and (4) that $\mathbf{D}_I$ satisfies the wave equation

$$\nabla \times \nabla \times (\overleftrightarrow{\epsilon}^{-1} \cdot \mathbf{D}_I) - k_s^2 \mathbf{D}_I = \mathbf{0}, \tag{6}$$

with $k_s^2 = \omega^2 \epsilon_s \mu_s$ and

$$\overleftrightarrow{\epsilon}^{-1} = \begin{pmatrix} 1 & 0 & 0 \\ 0 & 1 & 0 \\ 0 & 0 & \dfrac{1}{1+u} \end{pmatrix}. \tag{7}$$

The divergenceless property (3c) suggests that $\mathbf{D}_I$ be expanded in terms of the vector spherical wave functions (VSWFs) $\mathbf{M}_{mn}^{(1)}(k,\mathbf{r})$ and $\mathbf{N}_{mn}^{(1)}(k,\mathbf{r})$ [21–23]

$$\mathbf{D}_I = \sum_{n,m} E_{mn}[c_{mn}\mathbf{M}_{mn}^{(1)}(k,\mathbf{r}) + d_{mn}\mathbf{N}_{mn}^{(1)}(k,\mathbf{r})], \tag{8}$$

where c_{mn} and d_{mn} are the expansion coefficients, and k is as yet undetermined. In general, there are three kinds of VSWFs: $\mathbf{M}_{mn}^{(J)}(k,\mathbf{r})$, $\mathbf{N}_{mn}^{(J)}(k,\mathbf{r})$, and $\mathbf{L}_{mn}^{(J)}(k,\mathbf{r})$. The divergenceless property of $\mathbf{D}$ implies that it does not involve $\mathbf{L}_{mn}$, thereby simplifying the algebra involved. The three kinds of VSWFs are defined for $J=1$ and 3 as in Refs. [21–23]. Except otherwise explicitly specified, hereinafter the summation $\Sigma_{n,m}$ implies that n runs from 1 to $+\infty$ and m from $-n$ to $+n$ for each n. The implication of $\Sigma_{\nu,\mu}$ is similar. The prefactor E_{mn} is given by $E_{mn} = i^n E_0 C_{mn}$, with E_0 characterizing the amplitude of the electric field of incident wave and [22]

$$C_{mn} = \left[\frac{2n+1}{n(n+1)} \frac{(n-m)!}{(n+m)!}\right]^{1/2}. \tag{9}$$

By using the properties of VSWFs, it can be worked out that [21]

$$\overleftrightarrow{\epsilon}^{-1} \cdot \mathbf{M}_{mn} = \sum_{\nu=0}^{+\infty} \sum_{\mu=-\nu}^{+\nu} [\tilde{g}_{\mu\nu}^{mn}\mathbf{M}_{\mu\nu} + \tilde{e}_{\mu\nu}^{mn}\mathbf{N}_{\mu\nu} + \tilde{f}_{\mu\nu}^{mn}\mathbf{L}_{\mu\nu}],$$

$$\overleftrightarrow{\epsilon}^{-1} \cdot \mathbf{N}_{mn} = \sum_{\nu=0}^{+\infty} \sum_{\mu=-\nu}^{+\nu} [\bar{g}_{\mu\nu}^{mn}\mathbf{M}_{\mu\nu} + \bar{e}_{\mu\nu}^{mn}\mathbf{N}_{\mu\nu} + \bar{f}_{\mu\nu}^{mn}\mathbf{L}_{\mu\nu}]. \tag{10}$$

Therefore, one has

$$\overleftrightarrow{\epsilon}^{-1}\cdot\mathbf{D}_I=\sum_{n,m}E_{mn}[\bar{c}_{mn}\mathbf{M}_{mn}^{(1)}(k,\mathbf{r})+\bar{d}_{mn}\mathbf{N}_{mn}^{(1)}(k,\mathbf{r})$$
$$+w_{mn}\mathbf{L}_{mn}^{(1)}(k,\mathbf{r})]+w_{00}\mathbf{L}_{00}^{(1)}(k,\mathbf{r}),\qquad(11)$$

where the coefficients $\tilde{g}_{\mu\nu}^{mn},\tilde{e}_{\mu\nu}^{mn},\tilde{f}_{\mu\nu}^{mn}$ etc., together with $\bar{d}_{mn}$, $\bar{c}_{mn}$, w_{mn}, and w_{00}, can be obtained in the same way as in Ref. [21].

Inserting (8) and (11) into the wave equation (6), after some algebra one gets

$$\sum_{n,m}E_{mn}[\tilde{c}_{mn}\mathbf{M}_{mn}^{(1)}(k,\mathbf{r})+\tilde{d}_{mn}\mathbf{N}_{mn}^{(1)}(k,\mathbf{r})]=\mathbf{0},\qquad(12)$$

with

$$\tilde{c}_{mn}=k^2\sum_{\nu,\mu}\frac{E_{\mu\nu}}{E_{mn}}[\tilde{g}_{mn}^{\mu\nu}c_{\mu\nu}+\bar{g}_{mn}^{\mu\nu}d_{\mu\nu}]-k_s^2c_{mn},$$

$$\tilde{d}_{mn}=k^2\sum_{\nu,\mu}\frac{E_{\mu\nu}}{E_{mn}}[\tilde{e}_{mn}^{\mu\nu}c_{\mu\nu}+\bar{e}_{mn}^{\mu\nu}d_{\mu\nu}]-k_s^2d_{mn}.\qquad(13)$$

Equations (12) and (13) imply an eigensystem governing the value of k for expansion (8)

$$\begin{pmatrix}\bar{\mathcal{E}} & \tilde{\mathcal{E}}\\ \bar{\mathcal{G}} & \tilde{\mathcal{G}}\end{pmatrix}\begin{pmatrix}d\\ c\end{pmatrix}=\lambda\begin{pmatrix}d\\ c\end{pmatrix},\qquad(14)$$

where $\lambda=k_s^2/k^2$, and the matrices $\tilde{\mathcal{G}}$, $\bar{\mathcal{G}}$, $\tilde{\mathcal{E}}$, and $\bar{\mathcal{E}}$ are given by

$$\tilde{\mathcal{G}}_{mn,\mu\nu}=\frac{E_{\mu\nu}}{E_{mn}}\tilde{g}_{mn}^{\mu\nu},\quad \bar{\mathcal{G}}_{mn,\mu\nu}=\frac{E_{\mu\nu}}{E_{mn}}\bar{g}_{mn}^{\mu\nu},$$

$$\tilde{\mathcal{E}}_{mn,\mu\nu}=\frac{E_{\mu\nu}}{E_{mn}}\tilde{e}_{mn}^{\mu\nu},\quad \bar{\mathcal{E}}_{mn,\mu\nu}=\frac{E_{\mu\nu}}{E_{mn}}\bar{e}_{mn}^{\mu\nu},\qquad(15)$$

with mn and $\mu\nu$ denoting the row and column indices, respectively. Let λ_l and $(d_{mn,l},c_{mn,l})^T$ denote, respectively, the eigenvalues and the corresponding eigenvectors of eigensystem (14), with l representing the index of eigenvalues and corresponding eigenvectors. One can then construct a new set of vector functions $\mathbf{V}_l$ based on the eigenvectors $(d_{mn,l},c_{mn,l})^T$

$$\mathbf{V}_l=-\frac{i\epsilon_s}{\lambda_l}\sum_{n,m}E_{mn}[c_{mn,l}\mathbf{M}_{mn}^{(1)}(k_l,\mathbf{r})+d_{mn,l}\mathbf{N}_{mn}^{(1)}(k_l,\mathbf{r})],\qquad(16)$$

with $k_l=k_s/\sqrt{\lambda_l}$. It follows directly from

$$\nabla\cdot\mathbf{M}_{mn}=\nabla\cdot\mathbf{N}_{mn}=0\qquad(17)$$

that $\mathbf{V}_l$ are divergenceless

$$\nabla\cdot\mathbf{V}_l=0.\qquad(18a)$$

In addition, they satisfy the wave equation for $\mathbf{D}_I$ field (6)

$$\nabla\times\nabla\times(\overleftrightarrow{\epsilon}^{-1}\cdot\mathbf{V}_l)-k_s^2\mathbf{V}_l=\mathbf{0}.\qquad(18b)$$

Thus, $\mathbf{D}_I$ can be expanded in terms of $\mathbf{V}_l$

$$\mathbf{D}_I=\sum_l\alpha_l\mathbf{V}_l,\qquad(19)$$

where the expansion coefficients α_l are to be determined by matching the boundary conditions at the surface of sphere. With $\mathbf{D}_I$ given by (19), it follows from (3a) and (4) that $\mathbf{E}_I$ and $\mathbf{H}_I$ fields can be written as

$$\mathbf{E}_I=\frac{1}{\epsilon_s}\overleftrightarrow{\epsilon}^{-1}\cdot\mathbf{D}_I=-\sum_{n,m}iE_{mn}\sum_l\alpha_l\Bigg[c_{mn,l}\mathbf{M}_{mn}^{(1)}(k_l,\mathbf{r})+d_{mn,l}$$
$$\times\mathbf{N}_{mn}^{(1)}(k_l,\mathbf{r})+\frac{w_{mn,l}}{\lambda_l}\mathbf{L}_{mn}^{(1)}(k_l,\mathbf{r})\Bigg]$$
$$+\sum_l i\alpha_l\left[\frac{w_{00,l}}{\lambda_l}\mathbf{L}_{00}^{(1)}(k_l,\mathbf{r})\right],$$

$$\mathbf{H}_I=\frac{-i}{\omega\mu_s}\nabla\times\mathbf{E}_I=-\frac{1}{\omega\mu_s}\sum_{n,m}E_{mn}\sum_l k_l\alpha_l[d_{mn,l}\mathbf{M}_{mn}^{(1)}(k_l,\mathbf{r})$$
$$+c_{mn,l}\mathbf{N}_{mn}^{(1)}(k_l,\mathbf{r})],\qquad(20)$$

with

$$w_{mn,l}=\sum_{\nu,\mu}\frac{E_{\mu\nu}}{E_{mn}}[\bar{f}_{mn}^{\mu\nu}d_{\mu\nu,l}+\tilde{f}_{mn}^{\mu\nu}c_{\mu\nu,l}],$$

$$w_{00,l}=\sum_{\nu,\mu}E_{\mu\nu}[\bar{f}_{00}^{\mu\nu}d_{\mu\nu,l}+\tilde{f}_{00}^{\mu\nu}c_{\mu\nu,l}]=-\sqrt{\frac{2}{15}}ud_{02,l}.$$

Notice that, since $\mathbf{E}_I$ no longer satisfies $\nabla\cdot\mathbf{E}_I=0$, its expansion includes $\mathbf{L}_{mn}$ terms that are absent in the isotropic case.

The scattered fields $\mathbf{E}_s$, $\mathbf{H}_s$, and incident fields $\mathbf{E}_{\rm inc}$, $\mathbf{H}_{\rm inc}$ in the isotropic surrounding medium have the same form as in the Mie solution [23,24]. However, since the form of the permittivity tensor adopted [see (5)] implies that the EA of birefringent particle is along the z axis, for arbitrary incident direction of plane wave, the expansions of the field are not limited to $m=\pm1$ modes.

In terms of VSWFs, the scattered fields $(\mathbf{E}_s,\mathbf{H}_s)$ are expanded as

$$\mathbf{E}_s=\sum_{n,m}iE_{mn}[a_{mn}\mathbf{N}_{mn}^{(3)}(k_0,\mathbf{r})+b_{mn}\mathbf{M}_{mn}^{(3)}(k_0,\mathbf{r})],$$

$$\mathbf{H}_s=\frac{k_0}{\omega\mu_0}\sum_{n,m}E_{mn}[b_{mn}\mathbf{N}_{mn}^{(3)}(k_0,\mathbf{r})+a_{mn}\mathbf{M}_{mn}^{(3)}(k_0,\mathbf{r})],\quad(21)$$

where $k_0^2=\omega^2\epsilon_0\mu_0$ with ϵ_0 and μ_0 being, respectively, the scalar permittivity and permeability of the surrounding medium. The expansion coefficients a_{mn} and b_{mn} are to be determined by matching boundary conditions.

Suppose that the particle is illuminated by a plane wave characterized by the incident wave vector $\mathbf{k}_0$, with

$$\mathbf{k}_0=k_0(\sin\theta_k\cos\phi_k\mathbf{e}_x+\sin\theta_k\sin\phi_k\mathbf{e}_y+\cos\theta_k\mathbf{e}_z),\qquad(22)$$

where $\mathbf{e}_x$, $\mathbf{e}_y$, and $\mathbf{e}_z$ are three unit base vectors of the Cartesian coordinate system and $\theta_k(\phi_k)$ is the polar (azimuthal) angle of $\mathbf{k}_0$, as schematically shown in Fig. 1. The electric and magnetic fields of the incident plane wave are then

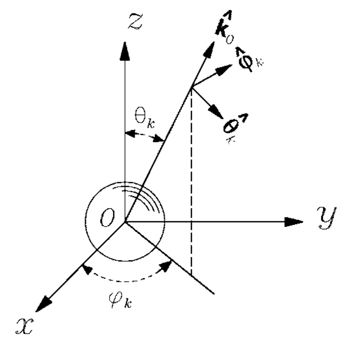

FIG. 1. Geometry of the scattering problem.

$$\mathbf{E}_{\mathrm{inc}} = E_0(p_\theta \hat{\boldsymbol{\theta}}_k + p_\phi \hat{\boldsymbol{\phi}}_k) e^{i\mathbf{k}_0\cdot\mathbf{r}},$$

$$\mathbf{H}_{\mathrm{inc}} = \frac{k_0}{\omega\mu_0} E_0(p_\theta \hat{\boldsymbol{\phi}}_k - p_\phi \hat{\boldsymbol{\theta}}_k) e^{i\mathbf{k}_0\cdot\mathbf{r}}, \tag{23}$$

where $\hat{\mathbf{p}}=(p_\theta\hat{\boldsymbol{\theta}}_k+p_\phi\hat{\boldsymbol{\phi}}_k)$ is the normalized complex polarization vector, with $|\hat{\mathbf{p}}|=1$, and the unit vectors $\hat{\boldsymbol{\theta}}_k$ and $\hat{\boldsymbol{\phi}}_k$ are defined in the direction of increasing θ_k and ϕ_k such as to constitute a right-hand base system together with $\hat{\mathbf{k}}_0=\mathbf{k}_0/k_0$, as shown in Fig. 1, namely

$$\hat{\mathbf{k}}_0 \times \hat{\boldsymbol{\theta}}_k = \hat{\boldsymbol{\phi}}_k, \quad \hat{\boldsymbol{\theta}}_k \times \hat{\boldsymbol{\phi}}_k = \hat{\mathbf{k}}_0, \quad \hat{\boldsymbol{\phi}}_k \times \hat{\mathbf{k}}_0 = \hat{\boldsymbol{\theta}}_k. \tag{24}$$

In terms of VSWFs, the incident fields $(\mathbf{E}_{\mathrm{inc}},\mathbf{H}_{\mathrm{inc}})$ read

$$\mathbf{E}_{\mathrm{inc}} = -\sum_{n,m} iE_{mn}[p_{mn}\mathbf{N}_{mn}^{(1)}(k_0,\mathbf{r}) + q_{mn}\mathbf{M}_{mn}^{(1)}(k_0,\mathbf{r})],$$

$$\mathbf{H}_{\mathrm{inc}} = -\frac{k_0}{\omega\mu_0}\sum_{n,m} E_{mn}[q_{mn}\mathbf{N}_{mn}^{(1)}(k_0,\mathbf{r}) + p_{mn}\mathbf{M}_{mn}^{(1)}(k_0,\mathbf{r})]. \tag{25}$$

The expansion coefficients p_{mn} and q_{mn} are

$$p_{mn} = [p_\theta \tilde{\tau}_{mn}(\cos\theta_k) - ip_\phi \tilde{\pi}_{mn}(\cos\theta_k)]e^{-im\phi_k},$$

$$q_{mn} = [p_\theta \tilde{\pi}_{mn}(\cos\theta_k) - ip_\phi \tilde{\tau}_{mn}(\cos\theta_k)]e^{-im\phi_k}, \tag{26}$$

where the regular angular functions $\tilde{\pi}_{mn}(\cos\theta)$ and $\tilde{\tau}_{mn}(\cos\theta)$ are defined based on the first kind of associated Legendre functions $P_n^m(\cos\theta)$ [22–24]

$$\tilde{\pi}_{mn}(\cos\theta) = C_{mn}\pi_{mn}(\cos\theta) = C_{mn}\frac{m}{\sin\theta}P_n^m(\cos\theta),$$

$$\tilde{\tau}_{mn}(\cos\theta) = C_{mn}\tau_{mn}(\cos\theta) = C_{mn}\frac{d}{d\theta}P_n^m(\cos\theta), \tag{27}$$

with C_{mn} defined in (9).

Matching boundary conditions at the surface of sphere, and after some algebra, one arrives at the equations that serve to determine the expansion coefficients α_l, a_{mn}, and b_{mn} based on p_{mn} and q_{mn}

$$\frac{1}{m_s}\sum_l \frac{1}{\bar{k}_l\lambda_l} j_n(\bar{k}_l m_s\eta) w_{mn,l}\alpha_l + \xi_n'(\eta)a_{mn} + \frac{1}{m_s}\sum_l \frac{1}{\bar{k}_l}\psi_n'(\bar{k}_l m_s\eta)d_{mn,l}\alpha_l = \psi_n'(\eta)p_{mn},$$

$$\xi_n(\eta)b_{mn} + \frac{1}{m_s}\sum_l \frac{1}{\bar{k}_l}\psi_n(\bar{k}_l m_s\eta)c_{mn,l}\alpha_l = \psi_n(\eta)q_{mn},$$

$$\xi_n(\eta)a_{mn} + \frac{\mu_0}{\mu_s}\sum_l \psi_n(\bar{k}_l m_s\eta)d_{mn,l}\alpha_l = \psi_n(\eta)p_{mn},$$

$$\xi_n'(\eta)b_{mn} + \frac{\mu_0}{\mu_s}\sum_l \psi_n'(\bar{k}_l m_s\eta)c_{mn,l}\alpha_l = \psi_n'(\eta)q_{mn}, \tag{28}$$

where

$$\eta = k_0 a, \quad m_s = \sqrt{1+u}\frac{k_s}{k_0}, \quad \bar{k}_l = \frac{k_l}{k_s}, \quad \lambda_l = \frac{k_s^2}{k_l^2} = \frac{1}{\bar{k}_l^2}, \tag{29}$$

with a the radius of spherical particle. The Riccati-Bessel functions $\psi_n(z), \xi_n(z), \chi_n(z)$ are given by [24]

$$\psi_n(z) = zj_n(z), \quad \xi_n(z) = zh_n^{(1)}(z), \quad \chi_n(z) = -zy_n(z). \tag{30}$$

Some details about numerical solution of (28) can be found in Ref. [21].

B. Radiation torque

With the incident fields and the scattered field given by (25) and (21), respectively, the total external field outside the particle reads

$$\mathbf{E}_e = \sum_{n,m} iE_{mn}[a_{mn}\mathbf{N}_{mn}^{(3)}(k_0,\mathbf{r}) + b_{mn}\mathbf{M}_{mn}^{(3)}(k_0,\mathbf{r}) - p_{mn} \times\mathbf{N}_{mn}^{(1)}(k_0,\mathbf{r}) - q_{mn}\mathbf{M}_{mn}^{(1)}(k_0,\mathbf{r})],$$

$$\mathbf{H}_e = \frac{k_0}{\omega\mu_0}\sum_{n,m} E_{mn}[b_{mn}\mathbf{N}_{mn}^{(3)}(k_0,\mathbf{r}) + a_{mn}\mathbf{M}_{mn}^{(3)}(k_0,\mathbf{r}) - q_{mn} \times\mathbf{N}_{mn}^{(1)}(k_0,\mathbf{r}) - p_{mn}\mathbf{M}_{mn}^{(1)}(k_0,\mathbf{r})], \tag{31}$$

which is explicitly reduced to

$$\mathbf{E}_e = \frac{i}{k_0 r}\sum_{n,m} E_{mn}e^{im\phi}\left[\frac{n(n+1)}{k_0 r}\mathcal{U}_{mn}P_n^m\mathbf{e}_r + (\mathcal{U}_{mn}'\tau_{mn} + \mathcal{V}_{mn}i\pi_{mn})\mathbf{e}_\theta + (\mathcal{U}_{mn}'i\pi_{mn} - \mathcal{V}_{mn}\tau_{mn})\mathbf{e}_\phi\right],$$

$$\mathbf{H}_e = \frac{k_0}{\omega\mu_0}\frac{1}{k_0 r}\sum_{n,m} E_{mn} e^{im\phi}\left[\frac{n(n+1)}{k_0 r}\mathcal{V}_{mn}P_n^m \mathbf{e}_r + (\mathcal{V}'_{mn}\tau_{mn} + \mathcal{U}_{mn} i\pi_{mn})\mathbf{e}_\theta + (\mathcal{V}'_{mn} i\pi_{mn} - \mathcal{U}_{mn}\tau_{mn})\mathbf{e}_\phi\right], \tag{32}$$

where

$$\mathcal{U}_{mn} = a_{mn}\xi_n(k_0 r) - p_{mn}\psi_n(k_0 r),$$

$$\mathcal{U}'_{mn} = a_{mn}\xi'_n(k_0 r) - p_{mn}\psi'_n(k_0 r),$$

$$\mathcal{V}_{mn} = b_{mn}\xi_n(k_0 r) - q_{mn}\psi_n(k_0 r),$$

$$\mathcal{V}'_{mn} = b_{mn}\xi'_n(k_0 r) - q_{mn}\psi'_n(k_0 r). \tag{33}$$

The time-averaged Maxwell stress tensor is then, for isotropic medium

$$\hat{\mathbf{T}} = \tfrac{1}{2}\,\mathrm{Re}\Big[\mathbf{E}_e\mathbf{D}_e^* + \mathbf{H}_e\mathbf{B}_e^* - \tfrac{1}{2}(\mathbf{E}_e\cdot\mathbf{D}_e^* + \mathbf{H}_e\cdot\mathbf{B}_e^*)\hat{\mathbf{I}}\Big], \tag{34}$$

where the superscript $*$ denotes the complex conjugate, and $\hat{\mathbf{I}}$ is the unit dyadic. The time-averaged torque $\boldsymbol{\Gamma}$ on the spherical scatterer can be evaluated by [25,26]

$$\boldsymbol{\Gamma} = -\int\!\!\int d\mathbf{S}\cdot\hat{\mathbf{K}} = -\int\!\!\int [\mathbf{e}_r\cdot\hat{\mathbf{K}}]dS, \tag{35}$$

where $\mathbf{e}_r=\mathbf{r}/r$ is the unit vector in radial direction with $r=|\mathbf{r}|$, and the time-averaged angular momentum flux tensor $\hat{\mathbf{K}}$ reads [26]

$$\hat{\mathbf{K}} = \hat{\mathbf{T}}\cdot[\mathbf{r}\times\hat{\mathbf{I}}] = \hat{\mathbf{T}}\times\mathbf{r}. \tag{36}$$

As a result, the time-averaged torque becomes

$$\boldsymbol{\Gamma} = -\int\!\!\int [\mathbf{e}_r\cdot(\hat{\mathbf{T}}\times\mathbf{r})]dS = \int\!\!\int [\mathbf{r}\times(\hat{\mathbf{T}}\cdot\mathbf{e}_r)]dS = r^3\int\!\!\int \mathbf{e}_r\times[\hat{\mathbf{T}}\cdot\mathbf{e}_r]d\Omega. \tag{37}$$

After some algebra, the Cartesian components of the torque can be worked out as

$$\boldsymbol{\Gamma} = \mathrm{Re}\{[\Gamma_x^{(1)}+\Gamma_x^{(2)}]\mathbf{e}_x + [\Gamma_y^{(1)}+\Gamma_y^{(2)}]\mathbf{e}_y + [\Gamma_z^{(1)}+\Gamma_z^{(2)}]\mathbf{e}_z\}, \tag{38}$$

where

$$\Gamma_x^{(1)} = \frac{1}{2}r^3\epsilon_0^*\sum_{n,m}\sum_{\nu,\mu}[\mathcal{V}_{mn}\mathcal{U}_{\mu\nu}^*\mathcal{W}_{\tau p}^{(x)} - \mathcal{U}'_{mn}\mathcal{U}_{\mu\nu}^*\mathcal{W}_{\pi p}^{(x)}],$$

$$\Gamma_y^{(1)} = \frac{1}{2}r^3\epsilon_0^*\sum_{n,m}\sum_{\nu,\mu}[\mathcal{V}_{mn}\mathcal{U}_{\mu\nu}^*\mathcal{W}_{\tau p}^{(y)} - \mathcal{U}'_{mn}\mathcal{U}_{\mu\nu}^*\mathcal{W}_{\pi p}^{(y)}],$$

$$\Gamma_z^{(1)} = \frac{1}{2}r^3\epsilon_0^*\sum_{n,m}\sum_{\nu,\mu}[\mathcal{V}_{mn}\mathcal{U}_{\mu\nu}^*\mathcal{W}_{\tau p}^{(z)} - \mathcal{U}'_{mn}\mathcal{U}_{\mu\nu}^*\mathcal{W}_{\pi p}^{(z)}], \tag{39}$$

$$\Gamma_x^{(2)} = \frac{1}{2}r^3\frac{|\epsilon_0\mu_0|}{\mu_0}\sum_{n,m}\sum_{\nu,\mu}[\mathcal{U}_{mn}\mathcal{V}_{\mu\nu}^*\mathcal{W}_{\tau p}^{(x)} - \mathcal{V}'_{mn}\mathcal{V}_{\mu\nu}^*\mathcal{W}_{\pi p}^{(x)}],$$

$$\Gamma_y^{(2)} = \frac{1}{2}r^3\frac{|\epsilon_0\mu_0|}{\mu_0}\sum_{n,m}\sum_{\nu,\mu}[\mathcal{U}_{mn}\mathcal{V}_{\mu\nu}^*\mathcal{W}_{\tau p}^{(y)} - \mathcal{V}'_{mn}\mathcal{V}_{\mu\nu}^*\mathcal{W}_{\pi p}^{(y)}],$$

$$\Gamma_z^{(2)} = \frac{1}{2}r^3\frac{|\epsilon_0\mu_0|}{\mu_0}\sum_{n,m}\sum_{\nu,\mu}[\mathcal{U}_{mn}\mathcal{V}_{\mu\nu}^*\mathcal{W}_{\tau p}^{(z)} - \mathcal{V}'_{mn}\mathcal{V}_{\mu\nu}^*\mathcal{W}_{\pi p}^{(z)}], \tag{40}$$

where $\mathcal{W}_{\tau p}^{(x,y,z)}$ and $\mathcal{W}_{\pi p}^{(x,y,z)}$ are integrals involving two regular auxiliary angular functions $\pi_{mn}(\cos\theta)$ and $\tau_{mn}(\cos\theta)$ given in the Appendix.

It should be noted that the integrations in Eqs. (35) and (37) are over the outer surface of the spherical particle, so $\mathcal{U}_{mn}$, $\mathcal{U}'_{mn}$, $\mathcal{V}_{mn}$, and $\mathcal{V}'_{mn}$ given by Eq. (33), as well as $\Gamma_{x,y,z}^{(1,2)}$ given in (39) and (40), should be calculated at the sphere surface $r=a$. If so evaluated, the formulas for radiation torque Eqs. (38)–(40) hold for both absorbing and lossless surrounding medium. They are presented here for arbitrary isotropic surrounding medium. If the background medium is lossless, with both permittivity and permeability being real numbers, then the integration (35) can be performed at spherical surface with arbitrary radius $r>a$, due to conservation of momentum and angular momentum. As a result, the integration is usually evaluated in the limit $r\to\infty$ for lossless surrounding medium, where the field expressions become much simpler by using the asymptotical formulas for Riccati-Bessel functions

$$\xi_n(\rho)\sim(-i)^{n+1}\exp(i\rho),\quad \zeta_n(\rho)\sim i^{n+1}\exp(-i\rho),$$

$$\psi_n(\rho)\sim[\xi_n(\rho)+\zeta_n(\rho)]/2. \tag{41}$$

Substituting Eq. (41) into Eqs. (39) and (40), after some algebra, the expressions for torque can be considerably simplified for lossless medium. They are

$$\Gamma_x = \mathrm{Re}[\mathcal{N}_1],\quad \Gamma_y = \mathrm{Im}[\mathcal{N}_1],\quad \Gamma_z = \mathrm{Re}[\mathcal{N}_2], \tag{42}$$

where

$$\mathcal{N}_1 = \frac{2\pi\epsilon_0|E_0|^2}{k_0^3}\sum_{n,m}\rho_{mn}(\tilde{a}_{m,n}\tilde{a}_{m+1,n}^* + \tilde{b}_{m,n}\tilde{b}_{m+1,n}^* - \tilde{p}_{m,n}\tilde{p}_{m+1,n}^* - \tilde{q}_{m,n}\tilde{q}_{m+1,n}^*),$$

$$\mathcal{N}_2 = -\frac{2\pi\epsilon_0|E_0|^2}{k_0^3}\sum_{n,m} m(|\tilde{a}_{m,n}|^2 + |\tilde{b}_{m,n}|^2 - |\tilde{p}_{m,n}|^2 - |\tilde{q}_{m,n}|^2), \tag{43}$$

with $\rho_{mn}=[(n-m)(n+m+1)]^{1/2}$, whereas $\tilde{a}_{m,n}$, $\tilde{b}_{m,n}$, $\tilde{p}_{m,n}$, and $\tilde{q}_{m,n}$ are given by

$$\tilde{a}_{m,n} = a_{mn} - \frac{1}{2}p_{mn},\quad \tilde{p}_{mn} = \frac{1}{2}p_{mn},$$

$$\tilde{b}_{m,n} = b_{mn} - \frac{1}{2}q_{mn},\quad \tilde{q}_{mn} = \frac{1}{2}q_{mn}, \tag{44}$$

with a_{mn}, b_{mn}, p_{mn}, and q_{mn} being coefficients in Eq. (31). We note that similar expressions for lossless background medium were presented by several authors [27–30].

III. NUMERICAL RESULTS

We are now ready to present systematic numerical results. Except otherwise explicitly specified, the results shown are mostly for the case with $\epsilon_r=\epsilon_s/\epsilon_0=2.56$, roughly a typical value in most experiments. The material birefringence is thus due to the anisotropic parameter u. In our numerical calculation, the EA of the birefringent particle is set to be the z axis, without loss of generality. The axial symmetry of the permittivity (5) implies that the scattering is independent of the azimuthal angle ϕ_k of the incident wave vector $\mathbf{k}_0$. As a result, for simplicity, we set $\phi_k=0$, which means $\hat{\boldsymbol{\phi}}_k=\mathbf{e}_\mathbf{y}$ and $\mathbf{k}_0$ lies in the x-y plane. The radiation torque is a function of incident angle θ_k. In addition, as most experiments applied a laser beam with fixed incident wavelength while the size of the particle is changed (see, e.g., Ref. [16]), in our calculation the optical torque is presented in units of $2I_0\lambda^3/c$, with c the light velocity, λ the incident wavelength, and $I_0=\frac{1}{2}c\epsilon_0|E_0|^2$ the incident irradiance.

A. Oblique illumination

We first study the case of oblique illumination, namely, the case with $\mathbf{k}_0$ not normal to the EA of the birefringent particle. Three different polarization modes of the incident plane wave are considered: (i) the TM mode, in which $\hat{\mathbf{p}}=\hat{\boldsymbol{\theta}}_k$ and the electric vector vibrates in the incident plane; (ii) the transverse electric (TE) mode, in which $\hat{\mathbf{p}}=\hat{\boldsymbol{\phi}}_k$ and thus the magnetic vector vibrates in the incident plane; and (iii) the left circularly polarized (LCP) mode with $\hat{\mathbf{p}}=(1/\sqrt{2})(\hat{\boldsymbol{\theta}}_k+i\hat{\boldsymbol{\phi}}_k)$. The incident plane is defined by the EA and $\mathbf{k}_0$. We do not study the right circularly polarized incident mode, since its results can be easily inferred from those for the LCP mode by symmetry.

The typical dependence of the optical torque on the incident angle θ_k is shown, for $0\leqslant\theta_k\leqslant\pi/2$, in Fig. 2 at size parameter $\eta=k_0a=5$ with different values of birefringent parameter u. For $\pi/2\leqslant\theta_k\leqslant\pi$, one has $\Gamma_y(\theta_k)=-\Gamma_y(\pi-\theta_k)$ and $\Gamma_x(\theta_k)=\Gamma_x(\pi-\theta_k)$ by symmetry. For TM and LCP incident modes, the y component of the optical torque Γ_y is found to display similar θ_k dependence. When $u>0(u<0)$, corresponding to $n_e>n_o(n_e<n_o)$, Γ_y is negative (positive), indicating that the optical torque due to the TM incidence will align the EA with the direction parallel (normal) to the E field, and the CP incidence will make the EA parallel (normal) to the plane of the incident E field. Stable equilibrium is reached at $\theta_k=\pi/2(\theta_k=0)$ for the $u>0(u<0)$ case. For the TM incident wave, the angle between the EA (z axis) and the incident electric field is $\varphi_e=(\pi/2)-\theta_k$, as shown in Fig. 2. However, the maximum value of Γ_y does not occur at $\varphi_e=\theta_k=\pi/4$, but instead depends on the material birefringence (the anisotropy parameter u). This is different from the normal illumination case with $\mathbf{k}_0$ perpendicular to the EA, where the torque always reaches its maximum at $\varphi_e=\pi/4$ (see Fig. 5 below) independent of the value of u. For the TE case, Γ_y is much smaller than in the TM case, and the θ_k dependence becomes somewhat complicated, especially for large u, as can be seen in Fig. 2(b). For the case with $u=0.4$, e.g., Γ_y changes sign as θ_k goes from 0 to $\pi/2$, resulting in two stable equilibrium states at both $\theta_k=0$ and $\theta_k=\pi/2$, quite different from the case of $u=0.2$, where only $\theta_k=0$ is rotationally stable. While for the TE and TM cases, Γ_y is the only nonvanishing component of the radiation torque, for the LCP incidence, besides Γ_y, the incident wave also exerts a positive Γ_x on the particle, trying to make the EA rotate together with the E field. When η and u are not very large, the magnitude of Γ_x monotonically increases with the incident angle θ_k in the region from 0 to $\pi/2$, and reaches a maximum at $\theta_k=\pi/2$; then it decreases with θ_k in the region from $\pi/2$ to π due to symmetry $\Gamma_x(\theta_k)=\Gamma_x(\pi-\theta_k)$.

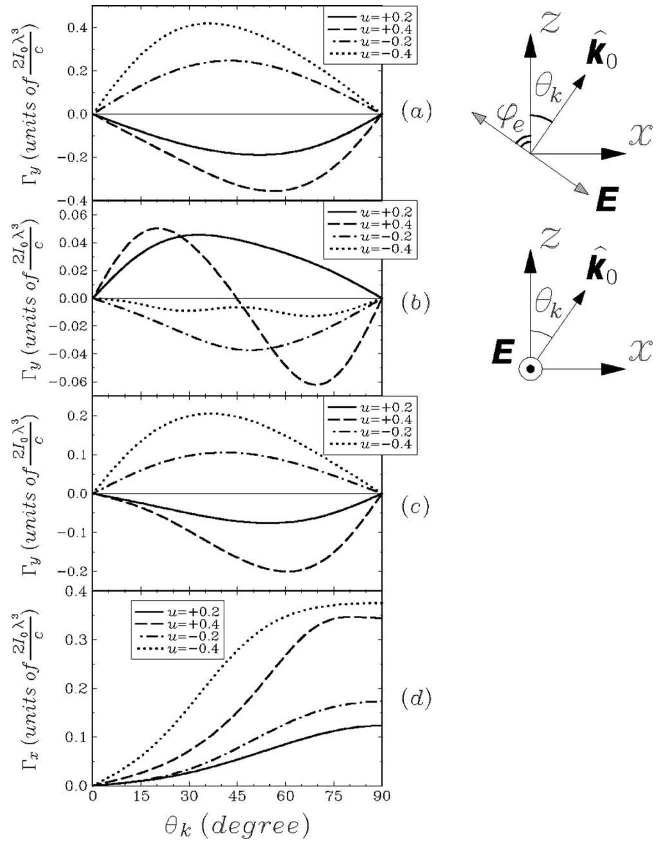

FIG. 2. The optical torque as a function of incident angle θ_k at $\eta=5$ and different values of birefringent anisotropy parameter u. (a) Γ_y versus θ_k for the TM incidence; (b) Γ_y versus θ_k for the TE incidence; (c) Γ_y versus θ_k for the LCP incidence; (d) Γ_x versus θ_k for the LCP incidence. Also shown are the schematic plots of the directions of incident wave vectors and E fields for the TM and the TE incidences.

Figure 3 shows Γ_y/η^3 and Γ_x/η^2 versus θ_k at $u=0.2$ for different values of size parameter η. Here, Γ_y/η^3 and Γ_x/η^2, instead of Γ_y and Γ_x, versus θ_k are exhibited for the convenience of displaying curves for different η in the same figure. For the TM and LCP incident waves, the θ_k dependence of Γ_y is similar to the case of small η, implying that, irrespective of the value of η, for the TM case, the optical torque always tends to make the EA parallel (normal) to the incident E field for particle with $n_e>n_o$ ($n_e<n_o$), and the LCP incidence will align the EA with the directions parallel (normal) to the E-field plane for particle with $n_e>n_o(n_e<n_o)$. For the

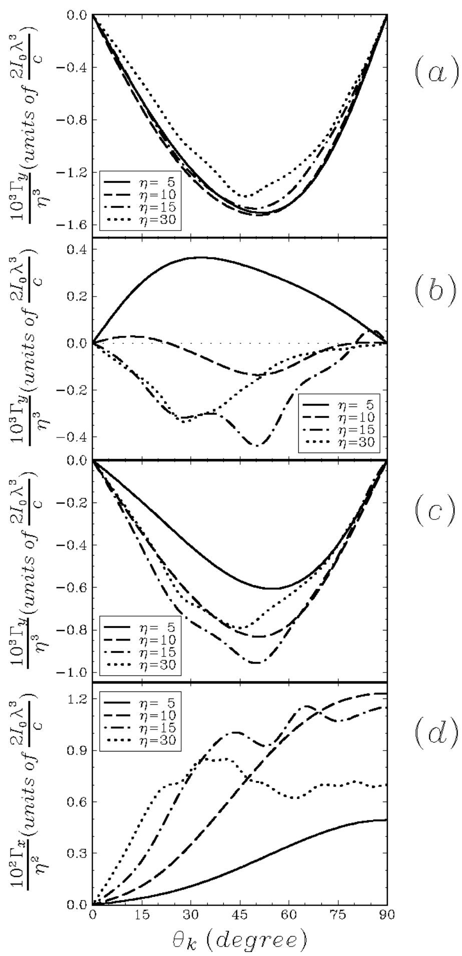

FIG. 3. Dependence of Γ_y/η^3 and Γ_x/η^2 on θ_k at u=0.2 and different values of η. (a) $10^3\Gamma_y/\eta^3$ versus θ_k for the TM incidence; (b) $10^3\Gamma_y/\eta^3$ versus θ_k for the TE incidence; (c) $10^3\Gamma_y/\eta^3$ versus θ_k for the LCP incidence; (d) $10^2\Gamma_x/\eta^2$ versus θ_k for the LCP incidence.

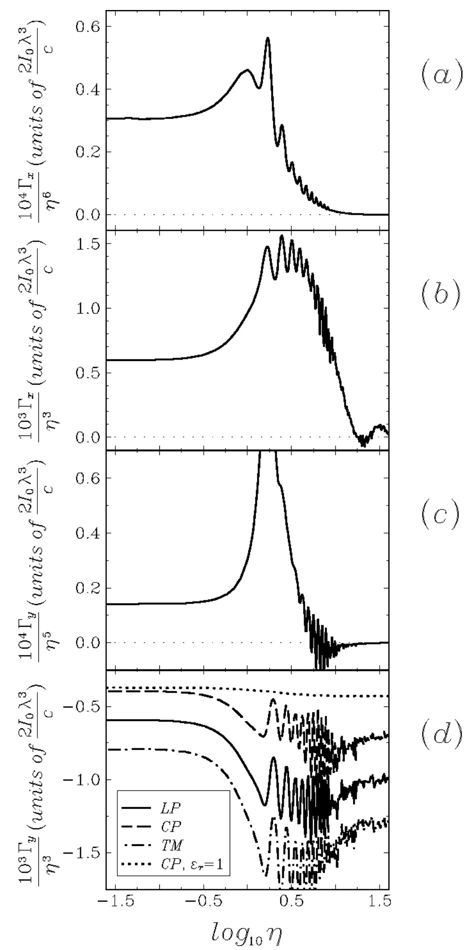

FIG. 4. (a) $10^4\Gamma_x/\eta^6$ versus $\log_{10}\eta$ at u=0.2 and incident angle θ_k=55° for the LCP incidence with $\hat{\mathbf{p}}=(1/\sqrt{2})(\hat{\boldsymbol{\theta}}_k+i\hat{\boldsymbol{\phi}}_k)$; (b) $10^3\Gamma_x/\eta^3$ versus $\log_{10}\eta$ at u=0.2 and θ_k=55° for the LP incidence with $\hat{\mathbf{p}}=\frac{1}{2}(\sqrt{3}\hat{\boldsymbol{\theta}}_k+\hat{\boldsymbol{\phi}}_k)$; (c) $10^4\Gamma_y/\eta^5$ versus $\log_{10}\eta$ at u=0.2 and θ_k=55° for the TE incidence with $\hat{\mathbf{p}}=\hat{\boldsymbol{\phi}}_k$; (d) $10^3\Gamma_y/\eta^3$ versus $\log_{10}\eta$ at u=0.2 and θ_k=55° for the LP, LCP, and TM incidences. Also shown as dotted line is $10^3\Gamma_y/\eta^3$ versus $\log_{10}\eta$ for the LCP case at matching case ϵ_r=1.

TE case, the θ_k dependence becomes complicated as η increases. For example, when η=5, θ_k=0 is the only rotationally stable equilibrium. For η=30, the only stable equilibrium is reached at $\theta_k=\pi/2$, in contrast to the case with η =5. If η=15, a stable equilibrium is achieved at $\theta_k\approx 80°$. Neither θ_k=0 nor $\theta_k=\pi/2$ is stable, although Γ_y vanishes at such values of θ_k. While η=10, both θ_k=0 and $\theta_k\approx 80°$ are stable. Finally, for the LCP case, the θ_k dependence of Γ_x is no longer monotonic in the region $0\leqslant\theta_k\leqslant\pi/2$ when η is large, as exhibited in Fig. 3(d) for η=15 and 30.

To study the particle size dependence of the optical torque in the small particle limit, we consider also the general LP incident mode, in addition to the TM, TE, and LCP modes. Here, the general LP mode is characterized by the polarization vector $\hat{\mathbf{p}}=p_\theta\hat{\boldsymbol{\theta}}_k+p_\phi\hat{\boldsymbol{\phi}}_k$, with both p_θ and p_ϕ real and neither p_θ nor p_ϕ vanishing. It is taken into account in order to address the particle size dependence of Γ_x, which is vanishing for both the TM (p_ϕ=0) and the TE (p_θ=0) cases. Both Γ_x and Γ_y versus particle size are found to exhibit different power laws for different incident polarization modes, as exemplified in Fig. 4 for θ_k=55° and u=0.2. Figure 4(a) and Fig. 4(b) display Γ_x/η^6 versus $\log_{10}\eta$ for the LCP incident wave and Γ_x/η^3 versus $\log_{10}\eta$ for the LP incident wave with $\hat{\mathbf{p}}=\frac{1}{2}(\sqrt{3}\hat{\boldsymbol{\theta}}_k+\hat{\boldsymbol{\phi}}_k)$, respectively. The flat curves at small η implies that $\Gamma_x\sim a^3$ for LP and $\Gamma_x\sim a^6$ for LCP incidences. Figure 4(c) and Fig. 4(d) show, respectively, the plots of Γ_y/η^5 and Γ_y/η^3 versus $\log_{10}\eta$ for the TE and other polarization modes studied. From Fig. 4(c), $\Gamma_y\sim a^5$ law is observed for the TE case, while Fig. 4(d) indicates that Γ_y obeys $\Gamma_y\sim a^3$ for all other incident polarization modes. In addition, although the $\Gamma_y\sim a^3$ law is violated for the nonmatching case at large η, our calculation shows that it still serves as a good approximation for the matching case ϵ_r=1 even for relatively large η, as can be seen from the dotted line in Fig. 4(d).

B. Normal illumination

Next, we turn to the normal illumination with incident $\mathbf{k}_0$ perpendicular to the EA, which has been intensively studied

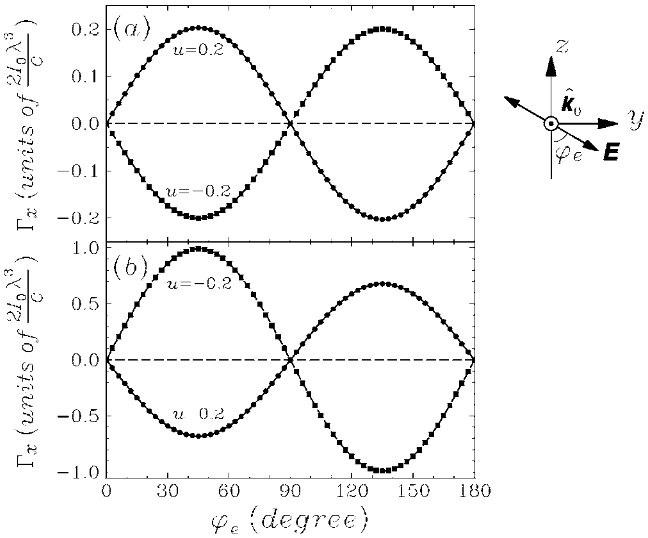

FIG. 5. Torque as a function of angle φ_e between the extraordinary axis and incident E field for normal illumination and $u=\pm 0.2$ at $\eta=5$ (a) and $\eta=15$ (b). The circles and squares are calculated results, while the lines represent $\Gamma_x=\Gamma_0 \sin 2\varphi_e$. Also shown is the schematic plot for the directions of incident wave vector and E field.

experimentally [12–19]. To be specific, the incident wave is characterized by (22) with $\theta_k=\pi/2$ and $\phi_k=0$, namely, $\mathbf{k}_0$ is in the x direction while keeping the EA in the z direction. For normal illumination, both the TE and the TM incident modes yield vanishing torque. We therefore consider two cases. The first case is the LP mode with the polarization vector given by $\hat{\mathbf{p}}=\cos\varphi_e\hat{\boldsymbol{\theta}}_k+\sin\varphi_e\hat{\boldsymbol{\phi}}_k=-\cos\varphi_e\mathbf{e}_z+\sin\varphi_e\mathbf{e}_y$, so that the angle between the EA and the incident E field is φ_e, as shown in Fig. 5. The TM and TE modes correspond to $\varphi_e=0$ and $\varphi_e=\pi/2$, respectively. The second case is the LCP incident wave with the polarization vector $\hat{\mathbf{p}}=(1/\sqrt{2})(\hat{\boldsymbol{\theta}}_k+i\hat{\boldsymbol{\phi}}_k)$.

Figure 5 shows the torque as a function of φ_e at $\eta=5$ and 15 for the LP incident wave. The circles and squares denote the calculated optical torque, while the lines represent $\Gamma_0 \sin 2\varphi_e$ curves, with Γ_0 the maximum magnitude of the torque. The sine dependence of torque on $2\varphi_e$ is found to hold up to numerical accuracy, with maximum magnitude of torque occurring at $\varphi_e=\pi/4$, as Eq. (2) proposed in Ref. [18] [see also the first term in (1)]. Our numerical results suggests that the $\Gamma_0 \sin 2\varphi_e$ law is valid for arbitrary size parameter η and material birefringence, provided that $\mathbf{k}_0$ is perpendicular to the EA. In addition, it is noted that when η is big enough, the EA of particle with $n_e>n_o(u>0)$ is aligned with the direction normal to the incident E field, in contrast with the case of small η experimentally studied [18]. This is clearly seen from Fig. 5. When $u=0.2$, the maximum magnitude of the torque $\Gamma_0>0$ for $\eta=5$, implying that the particle will rotate in the positive-x direction. The stable equilibrium is achieved at $\varphi_e=0$ or π, resulting in the alignment of the EA with the E field for $n_e>n_o$. For $u=-0.2$, $\Gamma_0<0$, a similar analysis leads to the conclusion that the EA is reoriented toward the direction normal to the E field for $n_e<n_o$. The situation becomes contrary for the case with $\eta=15$, as shown in Fig. 5(b), where $\varphi_e=0$ and π correspond to the stable equilibrium for $n_e<n_o$. For $n_e>n_o$, $\varphi_e=\pi/2$ is the stable equilibrium, implying that the optical torque tends to make the EA normal to the incident E field.

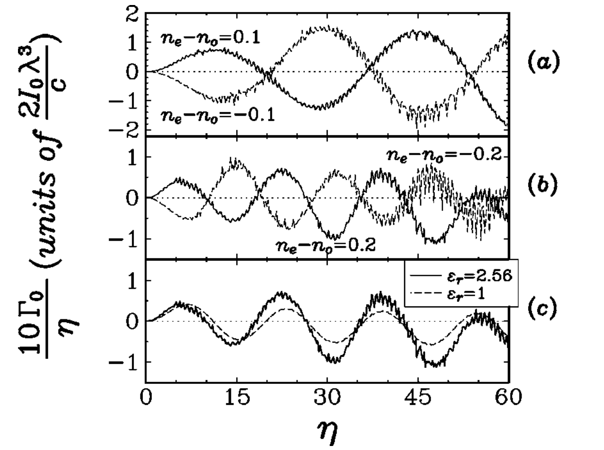

FIG. 6. $10\Gamma_0/\eta$ versus η for the LP normal illumination at (a) $n_e-n_o=\pm 0.1$; (b) $n_e-n_o=\pm 0.2$; and (c) $n_e-n_o=0.2$ with $\epsilon_r=1$ and 2.56.

Figure 6 shows Γ_0 for the LP incidence as a function of the size parameter η. It is found that, as the particle size increases, the torque will change its sign, implying that the particle with $n_e>n_o$ is not always aligned with the E field. In addition, Γ_0/η shows an overall wavelike behavior between positive and negative values, somewhat resembling the first term in (1) based on ray optics for a simple, ideally flat disk. In most cases, Γ_0 has different signs for $n_e-n_o=\pm|\Delta n|$, indicating that particles with $n_e-n_o=+|\Delta n|$ and $n_e-n_o=-|\Delta n|$ are subject to torque in opposite directions, which is in agreement with the first term in (1). However, it happens at some peculiar ranges of η that the torque may have the same sign for both $n_e-n_o=\pm|\Delta n|$, as shown, e.g., in Fig. 6(a) for $|\Delta n|=0.1$ at $\eta\sim 20$ and $\eta\sim 37$. This suggests that the EA may be aligned with the directions parallel or normal to the E field for both $n_e-n_o=\pm|\Delta n|$. The situation presents a striking contrast to the first term in (1), since the latter implies that the particles with $n_e-n_o=\pm|\Delta n|$ are always subject to torque in opposite directions. The difference comes from the effect of particle shape. Finally, it is also noted that the fluctuating behavior in Γ_x versus η curve is due to nonmatching $\epsilon_r\neq 1$. For the matching case $\epsilon_r=1$, the wavelike behavior becomes quite smooth, provided that $|\Delta n|$ is not very large, as can be seen in Fig. 6(c).

For the LCP incident wave, Fig. 7 shows plots of Γ_x/η^2 versus η for different material birefringences. Qualitative agreement is observed with the second term in (1). The difference lies in that the torque will never vanish except in the limit $\eta\to 0$, and the amplitude of the wavelike behavior decays with η at relative small η. The overall η dependence is similar to the LP case, except that Γ_x is always positive instead of fluctuating between positive and negative values in the LP case. This is because the LCP wave always transports positive angular momentum to the scatterer, while the LP wave can transfer both positive and negative angular momentum to the scatterer. In contrast to the LP case shown in

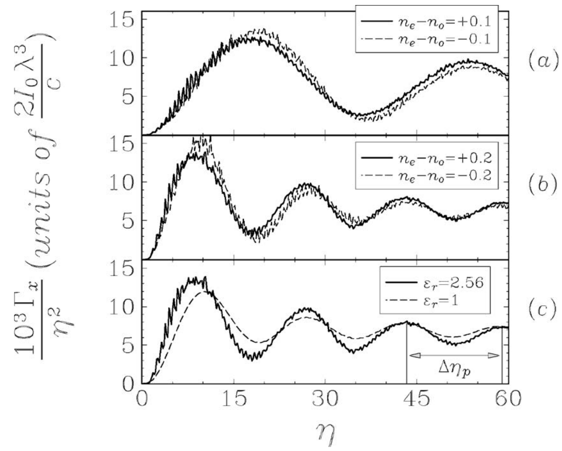

FIG. 7. $10^3\Gamma_x/\eta^2$ versus η for the LCP normal illumination at (a) $n_e-n_o=\pm 0.1$; (b) $n_e-n_o=\pm 0.2$; and (c) $n_e-n_o=0.2$ with $\epsilon_r=1$ and 2.56.

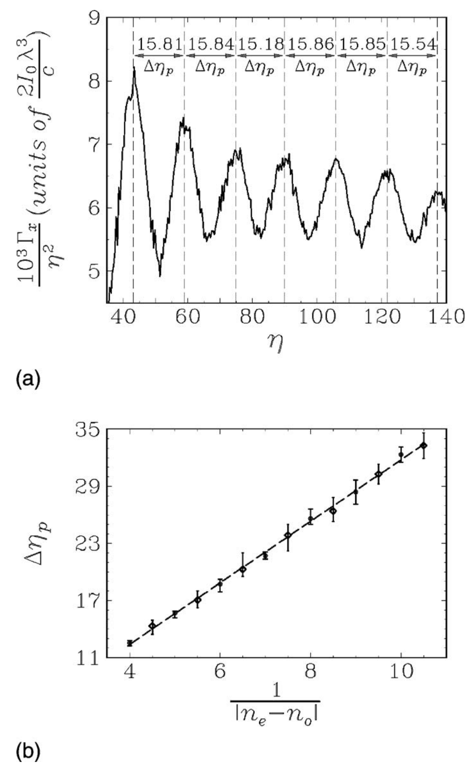

FIG. 8. (a) $10^3\Gamma_x/\eta^2$ versus η for the LCP normal illumination, showing that the peak separation $\Delta\eta_p$ fluctuates within only a few percent as η increases. (b) Peak separation $\Delta\eta_p$ as a function of $1/|n_e-n_o|$ at $\epsilon_r=2.56$. The error bars show the upper and lower bounds of $\Delta\eta_p$ as η goes from 40 to 140. The change of the material birefringence is due solely to the change in value of u. Filled circles are obtained for the case with $n_e>n_o$ and open diamonds for $n_e<n_o$. The dashed line is a guide to the eye showing the linear relation of $\Delta\eta_p$ versus $1/|n_e-n_o|$.

Fig. 6(a) and 6(b), for the LCP case, $n_e-n_o=\pm|\Delta n|$ yield quite similar results. And also, as in the LP case, the zigzag behavior is due to $\epsilon_r\neq 1$. When $\epsilon_r=1$, smooth wavelike dependence is observed, as shown in Fig. 7(c).

The wavelike behavior of Γ_x/η^2 versus η curve for the LCP incidence leads to the appearance of peaks as η increases, as shown in Fig. 7 and Fig. 8(a). The peak separation $\Delta\eta_p$ is dependent on $|n_e-n_o|$. In particular, it is found to fluctuate within 15% as η increases for all cases studied, as exemplified in Fig. 8(a). No decaying in amplitude of the wavelike behavior is found here for sufficiently large η. Figure 8(b) is a plot of peak separation $\Delta\eta_p$ as a function of $1/|n_e-n_o|$ for both $n_e>n_o$ and $n_o>n_e$. The error bars denote the upper and lower bounds of $\Delta\eta_p$ as η goes from 40 to 140. It is found that linear relation still provides a pretty fair approximation for $\Delta\eta_p$ versus $1/|n_e-n_o|$ irrespective of whether $n_e>n_o$ or $n_e<n_o$, in agreement with the second term in (1) as well as the experimental result [16]. The waveplate behavior is thus verified in the transfer of the angular momentum from the incident light to the scatterer.

To study dependence of the radiation torque on particle size in the small particle limit, Fig. 9 shows the plots of Γ_0/η^3 and Γ_x/η^6 versus $\log_{10}\eta$ for, respectively, the LP and LCP incident waves. An incident polarization-dependent scaling law is clearly exhibited: the torque due to the LP incidence obeys the scaling law $\Gamma_0\sim a^3$, as exhibited in Fig. 9(a) for some typical cases with $u=\pm 0.2$ and ± 0.4, while for the LCP incidence, the torque satisfies $\Gamma_x\sim a^6$, as shown typically in Fig. 9(b) for $u=\pm 0.2$ and ± 0.4.

Figure 10 displays the material birefringence dependence of the optical torque in the case of normal illumination for both the LP and the LCP incident modes. The change of the material birefringence is due solely to u while ϵ_r is kept at 2.56. For the LP incidence, we present results for Γ_x at $\varphi_e=\pi/4$, namely, Γ_0. The Γ/η^2 versus u, instead of Γ versus u, is displayed for the convenience of plotting curves for different values of η in the same figure. It is seen that there exists a monotonic increase region at small (absolute) value of u, in which the torque increases with the material birefringence, consistent with the experiment [16]. As $|u|$ increases, however, different oscillatory behaviors show up for different values of η, leading to appearance of many peaks in the range of u studied. As η increases, the monotonic increase region near $u=0$ shrinks, in qualitative agreement with (1). In addition, it is seen that Γ_x is always positive for the LCP incident wave. For the LP case, the torque may change its sign as the material birefringence increases, indicating that the EA of a birefringent particle with $n_e<n_o$ can also be oriented toward the E-field direction, even at relative small η, provided that the material birefringence is strong enough.

Figure 11 shows the typical torque versus the material birefringence behavior for small $|\Delta n|$. The torque due to the LP incident wave is found to display a linear dependence on $|\Delta n|$, while the torque by the CP incidence exhibits square law behavior $\Gamma\sim|\Delta n|^2$, both independent of the particle size. This dependence of Γ on Δn is in unexpected agreement with Eq. (1), although the latter is derived based on the ray optics for a flat disk.

Finally, in Fig. 12 the complex oscillatory behavior of Γ_0 versus $\epsilon_r=\epsilon_s/\epsilon_0$ is shown for the LP incidence at $u=\pm 0.2$ and different values of η. The appearance of sharp peaks recalls the Mie-type resonances. For small η, in the range of ϵ_s shown, it is seen that the torque does not change its sign. For large η, the torque may change its sign as ϵ_r increases.

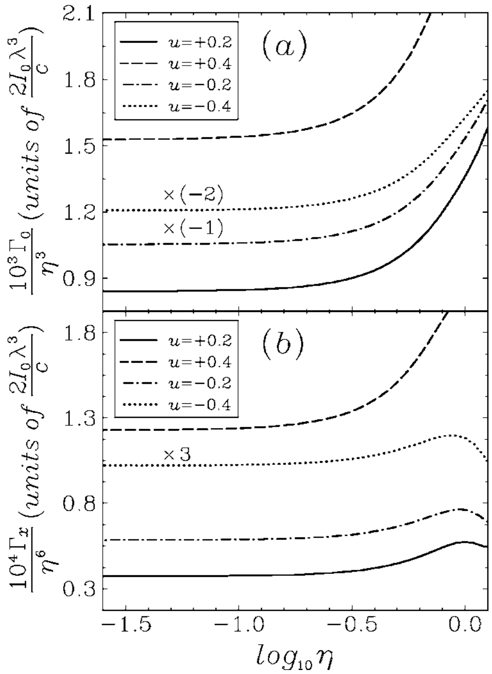

FIG. 9. (a) $10^3\Gamma_0/\eta^3$ versus $\log_{10}\eta$ at different values of u for the LP incidence; (b) $10^4\Gamma_x/\eta^6$ versus $\log_{10}\eta$ at different values of u for the LCP incidence. To fit all curves for different u in the same figure, results for the LP cases with $u=-0.2$ and $u=-0.4$ have been multiplied by -1 and $-\frac{1}{2}$, respectively, while the result for the LCP case with $u=-0.4$ has been multiplied by $\frac{1}{3}$.

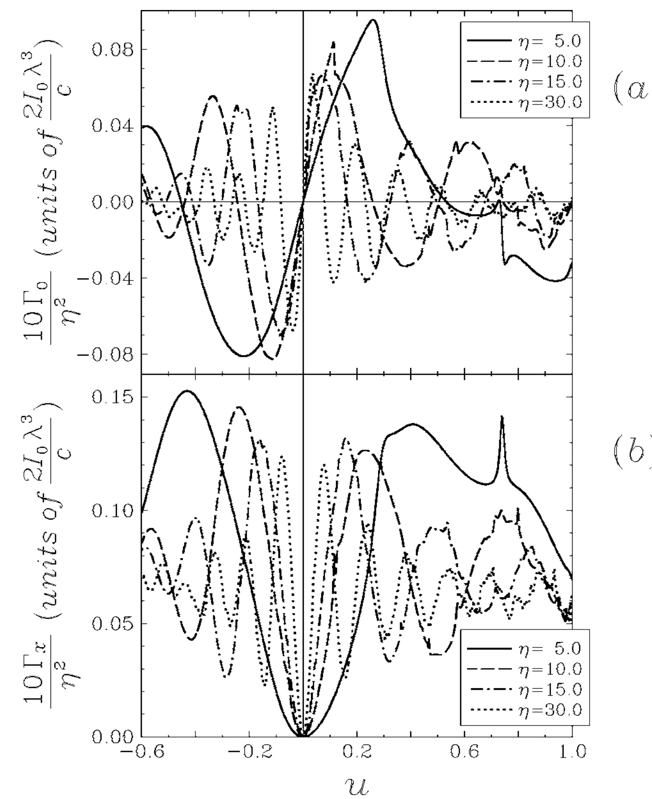

FIG. 10. The optical torque versus u at different values of η for the LP (a) and the LCP (b) normal illumination.

IV. SUMMARY

In summary, we have performed an exact *ab initio* calculation of the optical torque on a spherical birefringent particle of arbitrary size illuminated by plane electromagnetic wave with arbitrary polarization mode and direction of propagation, based on the extended Mie theory and the Maxwell stress tensor formalism. The expression for evaluating the radiation torque was derived for arbitrary (absorbing and lossless) isotropic surrounding medium. The radiation torque is found to exhibit miscellaneous dependences on the incident angle, the incident polarization, the material birefringence, as well as the particle size. The numerical results confirm the wave-plate mechanism in the transfer of angular momentum from the incident light to the scatterer. When a particle with $n_e>n_o$ ($n_e<n_o$) is subject to oblique illumination by a CP incident wave, its EA will always be aligned with the direction parallel (normal) to the E plane. An obliquely incident TM wave will reorient the EA of the scattering particle with $n_e>n_o$ ($n_e<n_o$) toward the direction parallel (normal) the incident E field irrespective of the particle size. When a particle is subject to normal illumination by a LP incident wave, the angle dependence (2), which is derived in the small particle limit, is found to hold for arbitrary particle size. The increase of the particle size affects only the value of Γ_0, making it vary between positive and negative numbers, indicating that even for a particle with $n_e>n_o$($n_e<n_o$), its EA is not always aligned with the direction parallel (normal) to the E field by the optical torque. Owing to the particle shape effect, in some peculiar ranges of η, the EA may be aligned with the E-field direction for both $n_e-n_o=|\Delta n|$ and $n_e-n_o=-|\Delta n|$, and vice versa, at some other ranges of η, the torque may cause a reorientation of the EA toward the direction normal to the E field, irrespective of $n_e-n_o=|\Delta n|$ or $n_e-n_o=-|\Delta n|$. In addition, dependent on the incident polarization mode as well as the incident direction, the radiation torque Γ exhibits different power-law dependences on the particle size in the small particle limit. To be specific, set the EA of the scattering particle to be the z axis and let the incident $\mathbf{k}_0$ be in x-z plane. For oblique illumination, Γ_x is found to satisfy $\Gamma_x\sim a^6$ and $\Gamma_x\sim a^3$ for the CP and the LP incidences, respectively, while Γ_y obeys $\Gamma_y\sim a^3$ for all incident polarization modes except the TE case, where Γ_y displays $\Gamma_y\sim a^5$ law, besides being much smaller than in other cases. For normal illumination, while Γ_y vanishes for any polarization mode, Γ_x behaves as in the case of oblique illumination, namely, $\Gamma\sim a^\alpha$, with the exponent $\alpha=3$ for the LP incidence and $\alpha=6$ for the CP incidence. Finally, when a particle with small material birefringence Δn is subject to normal LP and CP illuminations, the optical torque versus Δn displays linear and square law behaviors, respectively, regardless of the particle size.

Our direct classical calculation is merited due to subtleties of both classical and quantum theories of electromagnetic angular momentum. Furthermore, it is believed to be relevant to many applications where birefringent spherical particles are implemented, typically in the case of making measurements of viscosity on a microscopic scale [14]. We note that, in reality, the experiments on optical torque are performed using a laser beam. In most cases, however, the re-

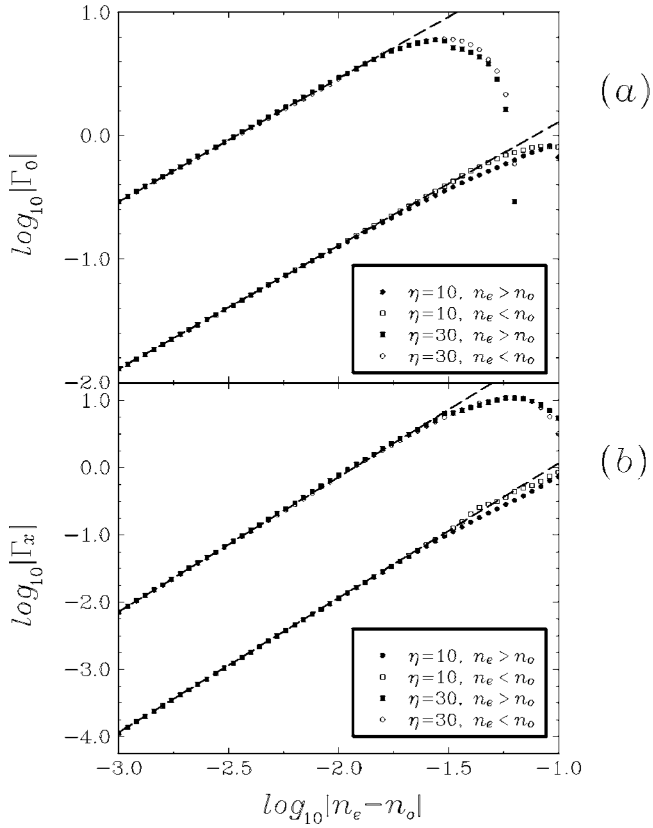

FIG. 11. The log-log plot of the optical torque versus the material birefringence $|\Delta n|$ at η=10 and 30 for the LP (a) and the LCP (b) normal illumination. The dashed lines are guides to the eye, showing $|\Gamma| \sim |\Delta n|$ and $|\Gamma| \sim |\Delta n|^2$ for the LP and the CP incident waves, respectively.

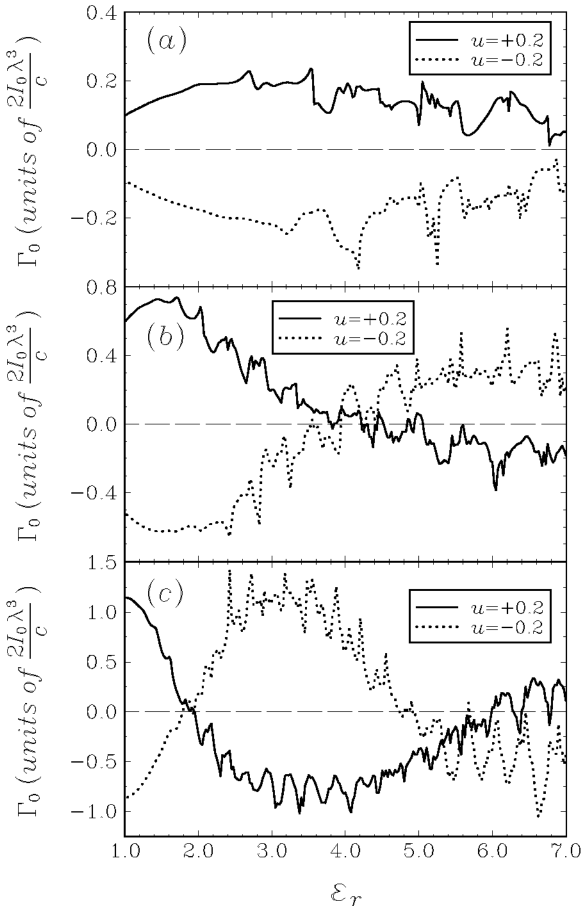

FIG. 12. Γ_0 versus $\epsilon_r = \epsilon_s/\epsilon_0$ for LP normal illumination at $u = \pm 0.2$ and η=5 (a), η=10 (b), and η=15 (c).

sults can be understood using the plane-wave picture [12], especially when the scattering particles are small compared with the beamwidth and located near the beam axis. In addition, our formulation provides a limiting case against which the solution of more complicated problems (e.g., torque on a particle illuminated by strongly focused laser beam) can be checked. Work along this line is in progress.

ACKNOWLEDGMENTS

M.L. and N.J. would like to thank Professor X.F. Ma for helpful discussion. The work is supported by CNKBRSF, China NNSF through 10474014 and 10321003, and PCSIRT.

APPENDIX: SOME INTEGRALS INVOLVING π_{mn} AND τ_{mn}

Two auxiliary functions, $\pi_{mn}(\cos\theta)$ and $\tau_{mn}(\cos\theta)$, are defined by

$$\pi_{mn}(\cos\theta) = \frac{m}{\sin\theta} P_n^m(\cos\theta),$$

$$\tau_{mn}(\cos\theta) = \frac{d}{d\theta} P_n^m(\cos\theta), \tag{A1}$$

where the first kind of associated Legendre function $P_n^m(x)$ is given by [22–24]

$$P_n^m(x) = \frac{1}{2^n n!}(1-x^2)^{m/2}\frac{d^{n+m}}{dx^{n+m}}[(x^2-1)^n]. \tag{A2}$$

The integrals $\mathcal{W}_{\tau p}^{(x,y,z)}$ and $\mathcal{W}_{\pi p}^{(x,y,z)}$ are

$$\begin{aligned}\mathcal{W}_{\pi p}^{(x)} &= \frac{v(v+1)}{|\eta|^2\eta^*} E_{mn}E_{\mu\nu}^* \int\int [i\pi_{mn}(\cos\theta)P_\nu^\mu(\cos\theta)\cos\theta\cos\phi + \tau_{mn}(\cos\theta)P_\nu^\mu(\cos\theta)\sin\phi]e^{i(m-u)\phi}d\Omega \\ &= i\frac{2\pi}{|\eta|^2\eta^*}|E_0|^2\{[(n-m)(v+u)]^{1/2}\delta_{v,n}\delta_{u,m+1} + [(n+m)(v-u)]^{1/2}\delta_{v,n}\delta_{u,m-1}\},\end{aligned}$$

$$\mathcal{W}_{\pi p}^{(y)}=\frac{v(v+1)}{|\eta|^2\eta^*}E_{mn}E_{\mu\nu}^*\int\int[i\pi_{mn}(\cos\theta)P_\nu^\mu(\cos\theta)\cos\theta\sin\phi-\tau_{mn}(\cos\theta)P_\nu^\mu(\cos\theta)\cos\phi]e^{i(m-u)\phi}d\Omega$$
$$=+\frac{2\pi}{|\eta|^2\eta^*}|E_0|^2\{[(n-m)(v+u)]^{1/2}\delta_{v,n}\delta_{u,m+1}-[(n+m)(v-u)]^{1/2}\delta_{v,n}\delta_{u,m-1}\},$$

$$\mathcal{W}_{\pi p}^{(z)}=-\frac{v(v+1)}{|\eta|^2\eta^*}E_{mn}E_{\mu\nu}^*\int\int i\pi_{mn}(\cos\theta)P_\nu^\mu(\cos\theta)e^{i(m-u)\phi}\sin\theta d\Omega=-i\frac{4m\pi}{|\eta|^2\eta^*}|E_0|^2\delta_{v,n}\delta_{u,m},$$

$$\mathcal{W}_{\tau p}^{(x)}=\frac{v(v+1)}{|\eta|^2\eta^*}E_{mn}E_{\mu\nu}^*\int\int[\tau_{mn}(\cos\theta)P_\nu^\mu(\cos\theta)\cos\theta\cos\phi-i\pi_{mn}(\cos\theta)P_\nu^\mu(\cos\theta)\sin\phi]e^{i(m-u)\phi}d\Omega$$
$$=i\frac{2\pi}{|\eta|^2\eta^*}|E_0|^2\left\{\left[\frac{(n^2-1)(n+m)(v+m)}{(2n+1)(2v+1)}\right]^{1/2}\delta_{v,n-1}\delta_{u,m-1}-\left[\frac{(v^2-1)(n-u)(v-u)}{(2n+1)(2v+1)}\right]^{1/2}\delta_{v,n+1}\delta_{u,m-1}\right.$$
$$\left.-\left[\frac{(n^2-1)(n-m)(v-m)}{(2n+1)(2v+1)}\right]^{1/2}\delta_{v,n-1}\delta_{u,m+1}+\left[\frac{(v^2-1)(n+u)(v+u)}{(2n+1)(2v+1)}\right]^{1/2}\delta_{v,n+1}\delta_{u,m+1}\right\},$$

$$\mathcal{W}_{\tau p}^{(y)}=\frac{v(v+1)}{|\eta|^2\eta^*}E_{mn}E_{\mu\nu}^*\int\int[\tau_{mn}(\cos\theta)P_\nu^\mu(\cos\theta)\cos\theta\sin\phi+i\pi_{mn}(\cos\theta)P_\nu^\mu(\cos\theta)\cos\phi]e^{i(m-u)\phi}d\Omega$$
$$=-\frac{2\pi}{|\eta|^2\eta^*}|E_0|^2\left\{\left[\frac{(n^2-1)(n+m)(v+m)}{(2n+1)(2v+1)}\right]^{1/2}\delta_{v,n-1}\delta_{u,m-1}-\left[\frac{(v^2-1)(n-u)(v-u)}{(2n+1)(2v+1)}\right]^{1/2}\delta_{v,n+1}\delta_{u,m-1}\right.$$
$$\left.+\left[\frac{(n^2-1)(n-m)(v-m)}{(2n+1)(2v+1)}\right]^{1/2}\delta_{v,n-1}\delta_{u,m+1}-\left[\frac{(v^2-1)(n+u)(v+u)}{(2n+1)(2v+1)}\right]^{1/2}\delta_{v,n+1}\delta_{u,m+1}\right\},$$

$$\mathcal{W}_{\tau p}^{(z)}=-\frac{v(v+1)}{|\eta|^2\eta^*}E_{mn}E_{\mu\nu}^*\int\int\tau_{mn}(\cos\theta)P_\nu^\mu(\cos\theta)e^{i(m-u)\phi}\sin\theta d\Omega$$
$$=i\frac{4\pi}{|\eta|^2\eta^*}|E_0|^2\left\{\left[\frac{(n^2-1)(n-m)(n+m)}{(2n+1)(2v+1)}\right]^{1/2}\delta_{v,n-1}\delta_{u,m}+\left[\frac{(v^2-1)(v-m)(v+m)}{(2n+1)(2v+1)}\right]^{1/2}\delta_{v,n+1}\delta_{u,m}\right\}.$$

[1] R. A. Beth, Phys. Rev. **50**, 115 (1936).
[2] A. Ashkin, Proc. Natl. Acad. Sci. U.S.A. **94**, 4853 (1997).
[3] P. L. Marston and J. H. Crichton, Phys. Rev. A **30**, 2508 (1984).
[4] M. E. J. Friese, J. Enger, H. Rubinsztein-Dunlop, and N. R. Heckenberg, Phys. Rev. A **54**, 1593 (1996).
[5] M. E. J. Friese, T. A. Nieminen, N. R. Heckenberg, and H. Rubinsztein-Dunlop, Opt. Lett. **23**, 1 (1998).
[6] S. Bayoudh, T. A. Nieminen, N. R. Heckenberg, and H. Rubinsztein-Dunlop, J. Mod. Opt. **50**, 1581 (2003).
[7] K. D. Bonin, B. Kourmanov, and T. G. Walker, Opt. Express **10**, 984 (2002).
[8] E. Santamato, A. Sasso, B. Piccirillo, and A. Vella, Opt. Express **10**, 871 (2002).
[9] Z. Cheng, P. M. Chaikin, and T. G. Mason, Phys. Rev. Lett. **89**, 108303 (2002).
[10] A. I. Bishop, T. A. Nieminen, N. R. Heckenberg, and H. Rubinsztein-Dunlop, Phys. Rev. A **68**, 033802 (2003).
[11] P. Galajda and P. Ormos, Opt. Express **11**, 446 (2003).
[12] M. E. J. Friese, T. A. Nieminen, N. R. Heckenberg, and H. Rubinsztein-Dunlop, Nature (London) **394**, 348 (1998); **395**, 621(E) (1998).
[13] E. Higurashi, R. Sawada, and T. Ito, Phys. Rev. E **59**, 3676 (1999).
[14] T. A. Nieminen, N. R. Heckenberg, and H. Rubinsztein-Dunlop, J. Mod. Opt. **48**, 405 (2001).
[15] M. E. J. Friese, H. Rubinsztein-Dunlop, J. Gold, P. Hagberg, and D. Hanstorp, Appl. Phys. Lett. **78**, 547 (2001).
[16] T. A. Wood, H. F. Gleeson, M. R. Dickinson, and A. J. Wright, Appl. Phys. Lett. **84**, 4292 (2004).
[17] S. Juodkazis, S. Matsuo, N. Murazawa, I. Hasegawa, and H. Misawa, Appl. Phys. Lett. **82**, 4657 (2003).
[18] A. La Porta and M. D. Wang, Phys. Rev. Lett. **92**, 190801 (2004).
[19] A. I. Bishop, T. A. Nieminen, N. R. Heckenberg, and H. Rubinsztein-Dunlop, Phys. Rev. Lett. **92**, 198104 (2004).
[20] A. Yu. Savchenko, N. V. Tabiryan, and B. Ya. Zeldovich, Phys. Rev. E **56**, 4773 (1997).
[21] Z. Lin and S. T. Chui, Phys. Rev. E **69**, 056614 (2004).
[22] Y. L. Xu, Appl. Opt. **34**, 4573 (1995); **36**, 9496 (1997); Phys. Lett. A **249**, 30 (1998); Phys. Rev. E **67**, 046620 (2003);

J. Opt. Soc. Am. A **20**, 2093 (2003).
[23] J. A. Stratton, *Electromagnetic Theory* (McGraw-Hill, New York, 1941).
[24] C. F. Bohren and D. R. Huffman, *Absorption and Scattering of Light by Small Particles* (John Wiley & Sons, New York 1983).
[25] J. D. Jackon, *Classical Electrodynamics*, 3rd ed. (Wiley, New York, 1999).
[26] J. Schwinger, L. L. DeRead, K. A. Milton, and W.-y. Tsai, *Classical Electrodynamics* (Perseus Books, Reading, MA 1998).
[27] S. Chang and S. S. Lee, J. Opt. Soc. Am. B **2**, 1853 (1985).
[28] J. P. Barton, D. R. Alexander, and S. A. Schaub, J. Appl. Phys. **66**, 4594 (1989).
[29] Ø. Farsund and B. U. Felderhof, Physica A **227**, 108 (1996).
[30] J. H. Crichton and P. L. Marston, Electron. J. Diff. Eqns., Proc. of Conf. 04, 37 (2000); available at http://www.ma.hw.ac.uk/EJDE/